Type of the Paper (Article)

Spectrally-selective energy-harvesting solar windows for public infrastructure and greenhouse applications

Mikhail Vasiliev*, Kamal Alameh and Mohammad Nur-E-Alam

Electron Science Research Institute (ESRI), Edith Cowan University, 270 Joondalup Dr, 6027, WA, Australia; E-mails: m.vasiliev@ecu.edu.au (M. V.) k.alameh@ecu.edu.au (K. A.), m.nur-e-alam@ecu.edu.au (M. N. A.)

* Correspondence: m.vasiliev@ecu.edu.au

Featured Application: Off-grid infrastructural installations powered by solar windows.

Abstract: A study of photovoltaic solar window technologies is reported, focusing on their structural features, functional materials, system development, and suitability for use in practical field applications, e.g. public infrastructures and agricultural installations. Energy generation performance characteristics are summarized and compared to theory-limit predictions. Working examples of pilot-trial solar window-based installations are described. We also report on achieving electric power outputs of about 25 W_p/m^2 from clear and transparent large-area glass-based solar windows.

Keywords: solar windows; advanced glazings; low-emissivity spectrally-selective coatings; photovoltaics

---

1. Introduction

In recent years, there has been a significant and growing research interest dedicated to the engineering and characterization of unconventional photovoltaic devices and systems, in particular, large-area transparent luminescent solar concentrators (LSC) [1-4], and solar windows [5-8], which are currently receiving increasing attention. Of special importance is the emergence of newly-commercialized semi-transparent photovoltaic technologies and building-integrated photovoltaic (BIPV) systems, which have been demonstrated in practical architectural deployment applications [9-12]. At present, most commercial energy-generating solar glass and solar window technologies suitable for BIPV applications feature semi-transparent (up to about 40% of spectrally-averaged visible-range transmission) appearance, and are most often not colour-neutral. This is due to typically relying on the use of either amorphous silicon-based, or dye-sensitized solar cell materials integrated into glass panel structures (in BIPV applications). In building-applied (BAPV) applications, the energy conversion is typically accomplished by either silicon, or CIS/CIGS solar cell modules embedded into, or onto, glass panels, building roofs, or façade walls. While such BAPV systems generate adequate electricity, their transparent area fraction is limited, often making them unattractive in architectural installations. A number of recent studies have been dedicated to uncovering the potential of renewable energy technologies (including photovoltaics) for reaching the important goal of net-zero energy consumption in buildings and infrastructural installations [13-18]. Figure 1 summarizes three well-known commercialized (and recent) examples of the relevant technologies, and also provides the data on the currently-available electric power generation capacities per unit wall area. Somewhat naturally, the electric outputs of solar window-type systems decrease with increasing visible-range transparency, regardless of the materials or technologies used. This is true for either the light concentrating or light-trapping (eg LSC) technologies, or the systems relying on solar cell-based direct wide-area PV conversion. The figure of 38 W_p/m^2 from Hanergy product manual [10] reported for a window panel of 40% averaged visible-range transparency appears to describe the top performance among all (or at least most) direct wide-area semitransparent glass-based energy converters available to date. This reported figure of performance is also well ahead (to the best of our knowledge) of all transparent concentrator-based window technologies or systems reported so far.

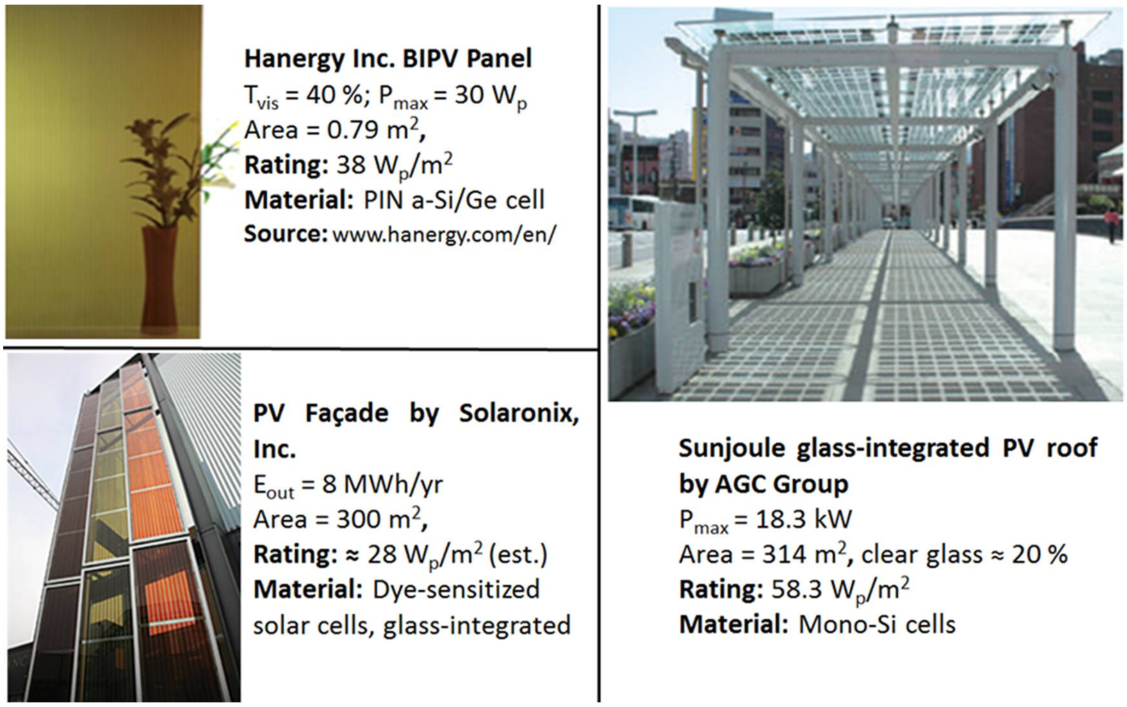

Figure 1. Commercial solar window technology examples [10, 11, 19] and their reported (or estimated) metrics in terms of energy-output characteristics.

A notable example of semitransparent photovoltaic façade installation engineered by Solaronix, Inc. and EPFL [19] is yet to undergo long-term performance characterization and testing, however, we can derive a figure of performance of about 28 W_P/m^2 of electric output, using the reported data on the predicted annual energy generation, the energy-converting area installed within the façade, and by approximating the other parameters (eg. using the reported 300 m^2 figure for the wall area, and by estimating 5 peak sunshine-hours per day, and about 190 sunny days per year).

Future BIPV technologies are widely expected to feature a combination of energy-saving functionality (due to superior thermal insulation properties provided by advanced glazing systems and low-emissivity coatings), and smart-window functionality offering active control over window transparency, together with a possibility of significant energy-harvesting performance available in increasingly high-transparency glazings [8, 9, 20]. The motivation for producing this article has been to highlight the emergence of a new class of highly-transparent solar windows, which are now ready for industrialization, and to compare the performance metrics of this emergent solar-window technology with other examples of solar window-type devices. We also aim at highlighting the actual potential of these solar windows for use in several practical applications.

2. Design features and performance characteristics of transparent solar windows

In order to ensure the energy-harvesting functionality in visibly-transparent concentrator-type windows, it is important to target specifically the non-visible parts of the solar spectrum (eg the UV and near-infrared (IR) spectral regions) in terms of both the light-trapping and also the energy-conversion functionalities. Therefore, the requirement for high visible-range transparency (and also the minimized haze) dictates the selection of all suitable functional materials, components, and structures for use within these advanced glazing systems. In particular, in concentrators relying on the LSC principle, the selection of luminophore materials is usually based on the requirement to harvest the energy within both the UV and also the near-IR spectral regions, and luminescent materials with large Stokes shift values are required to avoid excessive loss of light due to self-absorption [1-4, 7, 20, 21].

2.1 Materials and structures used within transparent energy-harvesting glazing systems

To efficiently convert the available near-IR energy (which, in spectrally-selective LSCs, is routed towards glass panel edges), it is very important to select the appropriate solar cell chemistry and solar module construction type, which will enable the photovoltaic conversion of this near-IR energy within the broadest possible spectral window, with the highest possible efficiency. Of particular importance for solar window applications is the selection of PV modules, which can maintain their efficiency (to the maximum extent possible) in the presence of significant adverse factors, such as transverse or longitudinal geometric shading from the incoming sunlight, as well as "spectral shading"- a condition in which the solar module is not illuminated by the full-spectrum sunlight, for which the selected PV module type was designed to operate. Despite the fact that the short-circuit current (I_{sc}) of any PV cell (or module) only depends on the incident optical power available at any given wavelength and the corresponding responsivity, the power-generation behaviour (and also the fill factor (FF) and efficiency) of PV modules connected to external electric loads becomes markedly more complicated in the presence of a combined influence of the geometric and spectral types of shading. These conditions are practically always encountered in concentrator-type solar window applications, where the cell modules are located at or near the glass panel edges, due to both the geometry of sunlight incidence and the device construction geometry itself. We found experimentally that the properties and performance of Avancis PowerMax 3.5 $CuInSe_2$ (CIS) PV modules were the most suitable for solar window applications, due to a large number of important technical considerations listed below:

- Broad spectral responsivity band of the CIS modules, which is a key factor for the design of visibly-transparent solar windows; their high efficiency (12.3%) is also a factor;
- The possibility of fitting the shape and size of CIS modules to the application requirements – by cutting and re-encapsulating the suitably-sized strips out of commercial CIS panels;
- A high degree of control over the electric circuit configuration performance in window modules. Also, the possibility of obtaining a high V_{oc} (up to about 50-55V) without extensive series connections;
- Mechanical robustness and reliability – the 2mm glass substrates are much more robust than mono-Si wafers;
- Superior (compared to many other cell types) performance of CIS modules in shading conditions and at elevated cell temperatures;
- The efficiency in factory-produced CIS cells has been increasing continuously in recent years.

Figure 2 shows the spectral responsivity of Avancis PV modules relative to the crystalline Si cells, and their external quantum efficiency (EQE) spectrum.

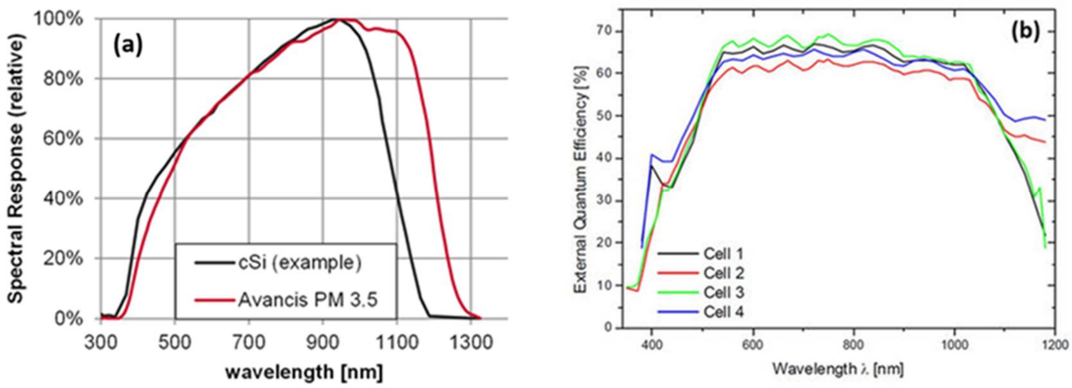

Preprints (www.preprints.org) | NOT PEER-REVIEWED | Posted: 2 May 2018 doi:10.20944/preprints201805.0016.v1

Peer-reviewed version available at Appl. Sci. 2018, 8, 849; doi:10.3390/app8060849

Figure 2. Avancis PowerMax 3.5 CIS cell modules' spectral performance characteristics. (a) Spectral responsivity curve measured relatively to the monocrystalline Si cells. These data are courtesy of Avancis, Inc. (Germany); (b) External Quantum Efficiency (EQE) of earlier Avancis CIS modules. These data are reproduced with permission from Ref [22].

Other spectrally-selective functional materials and glazing system components suitable for preferentially harvesting the non-visible parts of the solar spectrum energy in highly-transparent hybrid-type solar concentrators have been described in significant technical detail in [7] and [21]. For illustration and schematic purposes, Figure 3 outlines the main optical properties of glazing system components (the data of Figure 3 is reproduced from Ref. 7). The term "hybrid-type solar concentrator" refers to using simultaneously several types of physical mechanisms (eg luminescence, diffractive deflection, total internal reflection, and even scattering as a short-range light-trapping mechanism) - to promote the spectrally-selective concentration of light in near-edge regions of glazing-system panels. Using scattering, which in LSC field is generally known as a loss mechanism, as a (short-range) light-trapping mechanism working in conjunction with luminescence is a relatively new approach, discussed in some relevant detail within Refs. 6, 7, 21, and 23.

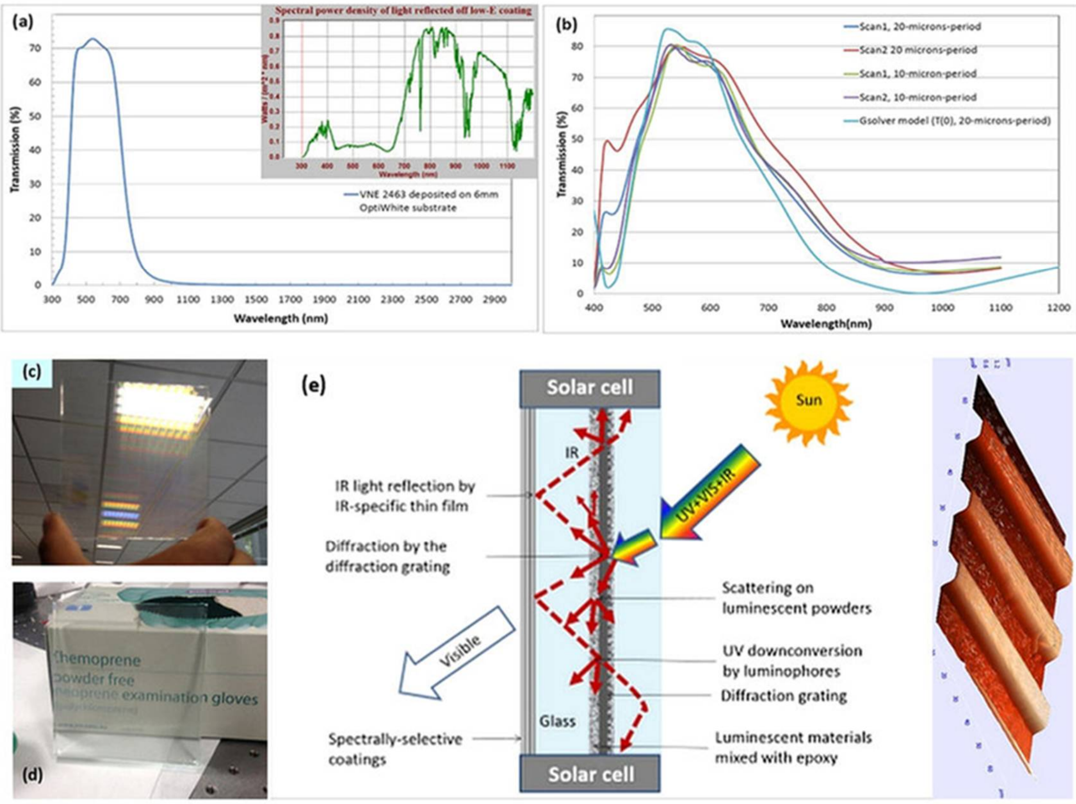

Figure 3. Components and structures used for constructing ClearVue PV window modules, and their main properties. Graphics is reproduced from Ref 7, for system structure illustration purposes. (a) Transmission spectrum of a high spectral selectivity low-e coating (Viracon, Inc. VNE 2463) and graph showing the spectral power density curve for the AM1.5G sunlight reflected off this coating; (b) Zero-order (direct) transmission of several transparent spectrally-selective diffraction grating samples measured using a spectrophotometer; (c) – (d) Visual appearance of either the unencapsulated, or the encapsulated diffraction grating; (e) overall schematic of an advanced transparent glazing system for energy harvesting concurrent with high thermal insulation, in which any internal air gap(s) are omitted for simplicity.

The main components which define both the visible transparency and the spectrally-selective energy harvesting properties of the glazing system are (i) the high-spectral-selectivity low-emissivity thin-film coating, and (ii) the visibly-transparent (when encapsulated using UV-curable epoxy and coverglass) spectrally-selective diffraction grating. The diffraction grating is designed to effectively

Preprints (www.preprints.org) | NOT PEER-REVIEWED | Posted: 2 May 2018 doi:10.20944/preprints201805.0016.v1

Peer-reviewed version available at *Appl. Sci.* **2018**, *8*, 849; doi:10.3390/app8060849

deflect the incident light in both the UV and the near-IR spectral ranges into multiple orders of transmission. The experimental methods suitable for the fabrication of suitable diffraction gratings are described in detail in [7]; the methods for the production of suitable types of optical thin-film coatings have been discussed in [24].

A unique combination of high-performance luminescent materials, which helps collect a large part of the incident UV energy and also a fraction of the incident near-IR energy from within a rather broad spectral region between about 900–1100 nm has been described in detail within the Supplementary dataset of [21]. Figure 4 (reproduced from Ref. 21) illustrates the functionality of a ZnS : (Ag, Tm)-based luminophore capable of efficiently converting the energy from a broad UV-blue wavelength range into a narrow emissions band centered at 794 nm, thus avoiding self-absorption losses.

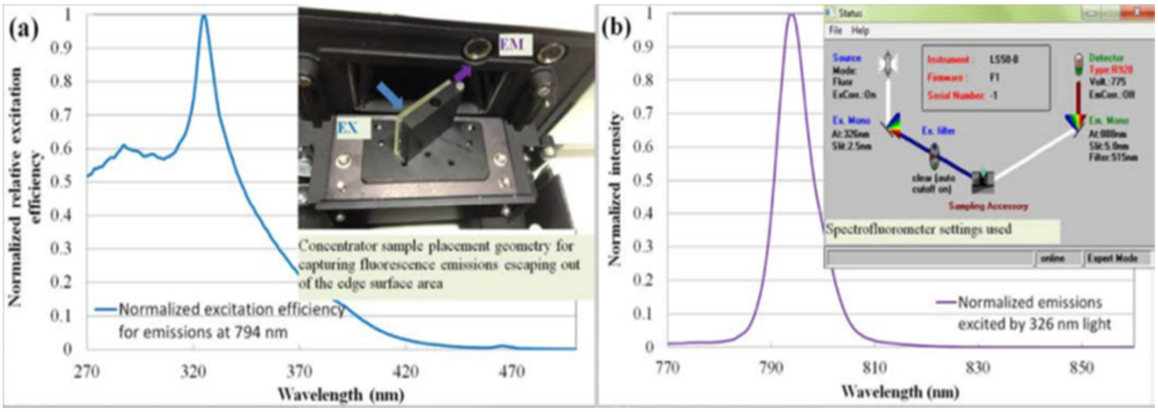

Figure 4. Measurements of the excitation and emission spectra of epoxy-based lamination interlayers containing suspended particles of ZnS : (Ag, Tm) luminophore. A Perkin-Elmer LS-50B luminescence spectrometer was used to collect and analyze the optical radiation flux propagating out of an edge area of 50x50x3mm^3 concentrator samples composed of two 1mm-thick Corning glass plates connected via a UV-cured functionalized epoxy interlayer. Luminophore particles were dispersed uniformly within liquid epoxy at concentrations not exceeding 1 wt%. Strong emission intensities were observed near 794 nm, almost saturating the spectrometer detection system, under normal-incidence UV excitation and when the sample edge area aperture was aligned with the input aperture of the emissions monochromator. This graphical dataset is reproduced from the Supplementary dataset of Ref 21.

Hybrid-type transparent planar solar concentrators employing the mechanisms of luminescence, scattering, and diffractive deflection of light form the basis of our approach to building practical solar windows suitable for architectural deployment. The apparent synergy between practically all of the above-named light-collection mechanisms (which is observed provided that the sizes and concentrations of all luminophore powder particles were selected carefully) was our significant finding, which governed the design of advanced glazings in multiple laboratory samples and factory-produced window modules.

2.2 Summary of solar windows performance and comparisons with theory limits

Two similar factory-assembled models of large-area (≈ 0.85 m^2) installation-ready framed solar windows were fabricated at Qingdao Rocky Ltd (China) in small test-run production batches during 2016-2017. Their performance characteristics varied slightly between window types, and from sample to sample, however, the electric power outputs per window started to approach about 20W in early samples produced industrially. Figure 5 shows solar windows during outdoor testing experiments (conducted in Perth, Australia, in May 2017) and the I-V curve measurement results. The measurements were conducted using PROVA 200A Solar Module Analyzer. The windows demonstrated their maximum electric power output when placed into a sun-facing near-vertical position, with a small (≈25°) tilt away from the vertical plane. The measurement results obtained were consistent with the expected weather-dependent autumn performance, and the observed orientation-angle dependency of output power (which yet to be characterized in detail and reported elsewhere)

Preprints (www.preprints.org) | NOT PEER-REVIEWED | Posted: 2 May 2018 doi:10.20944/preprints201805.0016.v1

Peer-reviewed version available at Appl. Sci. 2018, 8, 849; doi:10.3390/app8060849

was not significant. Rather large angular orientation changes applied to windows (up to 30-40 degrees in either direction away from the optimum orientation) in either the horizontal or vertical plane resulted typically in less than 20% of I_{sc} variations.

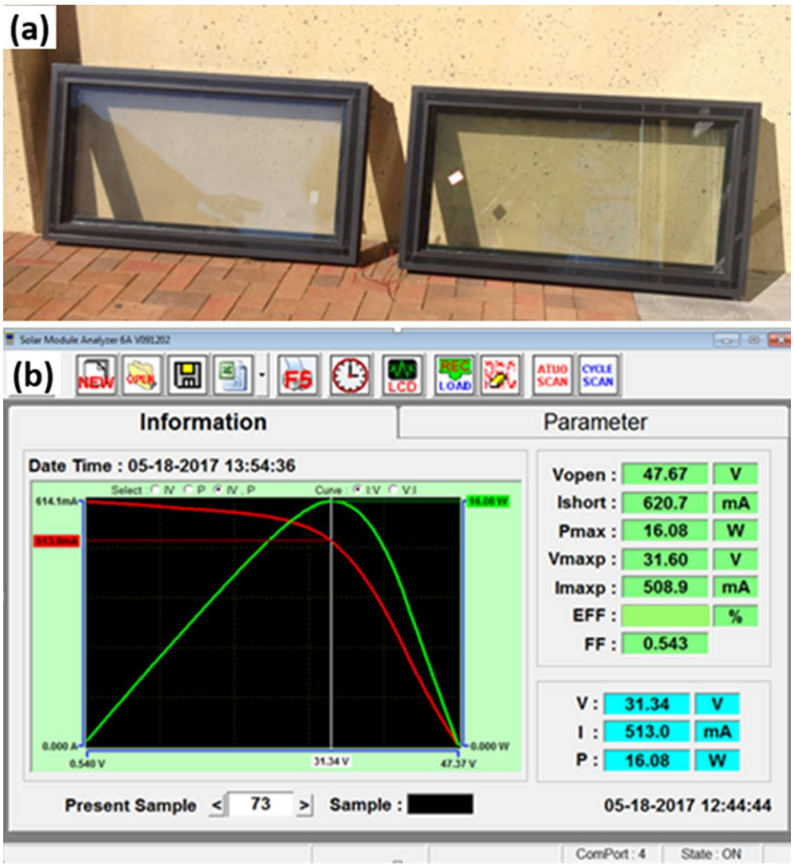

Figure 5. Solar windows constructed using glass panel dimensions of 1200 mm x 600 mm and their performance in autumn conditions. (a) Factory-assembled solar window samples; (b) Measured I-V curve data and electric output parameters. The measurements were performed on a hazy autumn day in Perth, with low UV index and solar irradiation intensity not exceeding 800 W/m^2, with sun-facing samples slightly tilted backwards from vertical position.

The window design features three parallel-connected solar-module (CIS) subsystems, each using stripe-shaped Avancis PowerMax 3.5 CIS circuit module cut-outs: (i) the edge-mounted modules, (ii) the backside perimeter-mounted modules, and (iii) external frame-mounted modules, which are used to stabilize the overall window-module operation and to achieve maximized energy-harvesting performance over the course of day. As is evident from the data of Figure 5, the overall module fill factor (MFF) of a solar window employing multiple interconnected CIS modules is significantly lower than the nominal FF (of near 0.66) of Avancis CIS products. This is largely due to the fact that each individual CIS module installed into a window receives substantially different amounts of illumination (and also shading), due to the variations in their geometric orientation with respect to the incoming sunlight, and also due to some shading caused by the framing system. Many individual CIS modules also differ in length (and thus the number of series-connected CIS cells), and therefore in V_{oc}. These variations lead to changes in the I-V curve shape features and affect the overall system FF, which in turn reduces the effective CIS-module efficiency compared to its nominal value.

A summary of measured window performance data obtained from another production batch of similarly-designed solar windows of total area 0.85 m^2 is shown in Table 1.

Peer-reviewed version available at *Appl. Sci.* **2018**, *8*, 849; doi:10.3390/app8060849

Table 1. Electric output summary and parameters of solar windows used in prototype bus-stop installation. The measurement conditions are described in detail, in order to provide an outlook on the potential usefulness of solar window products for use in different applications, versus using conventional PV modules.

Electric output parameters at peak	Measurement conditions / notes
• V_{oc} = 54-55 V • I_{sc} = 0.75-0.8 A • FF = 0.49-0.52 • P_{max} = (21.36 +/- 1.52) W_p • P_{max} ≈ 25-26 W_p/m^2	• Measurements performed in field conditions, on a very hot summer day. • Measurements made at near-peak weather and at near-peak window orientation and tilt. • The surface temperature of all CIS modules was > 40 °C. • Nominal CIS module efficiency 12.3%; nominal CIS module FF = 0.663. • Framed window area A_{tot} = 0.85 m^2; the total area of CIS cells installed A_{CIS} = 0.28 m^2. • Avancis PowerMax 3.5 130 CIS modules output nominally 97 W/m^2 at NOCT and AM 1.5 G. • External cells facing direct full-spectrum sunlight occupied 37% of the total A_{CIS} and contributed about 43% of total P_{max}; the edge-mounted cells occupied 29% of A_{CIS} and contributed 25.3% of P_{max}.

Each window within this batch had a glass panel area of 0.75 m^2 and external CIS modules area of 0.1 m^2. Due to cutting of original Avancis circuits, their re-encapsulation processes, and the overall factors affecting the window-module performance, the FF reduced from nominal 0.66 to ≈0.5, which effectively manifested in running all individual CIS cell modules at an averaged reduced efficiency of about 9.3%. The electrical mismatch losses within the window circuit partially resulted from a requirement to fit the external dimensions of windows to the required values, which affected the design features of the electric cirquitry through limitations imposed on the CIS cut-out lengths. The electric power output per 1 m^2 of the total framed window area reached about 25 W_p/m^2, and therefore approached about 26% of the nominal output available from 1m^2 of standard Avancis CIS module.

Theoretical performance limits for high-transparency window-type luminescent concentrators have been reported recently in [20]. An alternative way of calculating the same performance limit for an arbitrary level of window transparency presumes the idealized (complete) optical power collection of all available incident light by solar cells of known efficiency. Both calculations point to the same region of data for the maximum theoretical electric power output between 46-57 W_p/m^2 at T_{vis} = 70 %, if using CIS cells of 12.3 % nominal efficiency (and also by considering the Shockley-Queisser limit for CIGS cells if following the methodology of Ref. 20). This theory-limit performance is calculated for the peak geometric orientation and tilt of concentrator panels, at AM1.5G, 1000 W/m^2. The practically-achieved solar window performance (in factory-assembled framed window samples) is near 50 % of its theoretical limit. It is interesting to compare this result with the record-performing CIGS cells (η ≈ 20 %), which themselves operate at near 65 % of the Shockley-Queisser limit, as reported in [25].

3. Results

3.1 Principal results and future directions

The principal results of large-area solar window module development indicated that the technology of building transparent solar concentrator-type windows has now reached the stage, at which practical test-bedding applications within public infrastructure installations were feasible. Adshel Pty. Ltd. (Port Melbourne, Australia) has provided a public bus stop as a site for testing the applicability of ClearVue Technologies Ltd. solar windows for generating electric energy in self-

Preprints (www.preprints.org) | NOT PEER-REVIEWED | Posted: 2 May 2018 doi:10.20944/preprints201805.0016.v1

Peer-reviewed version available at Appl. Sci. 2018, 8, 849; doi:10.3390/app8060849

sustainable bus stops fitted with backlit advertising panels and LED lighting appliances. At the same time, ECU research team started considering the construction of a pilot greenhouse fitted with energy-generating clear windows. Figure 6 illustrates a range of previously-developed framed solar window types and highlights the differences in the optical transmission spectra of windows between two different application-area types (either the construction or agriculture industries). The core idea of using solar windows in new greenhouses is related to the possibility of spectrally tailoring the transmission spectra of glazing systems to the biological requirements of plants. The horticulturally-grown plants often favour the blue and red spectral regions for their illumination, in order to maximize crop productivity. We have adjusted the low-emissivity IR-reflector coating design techniques reported in [24] to fit the glazing-system transmission spectrum to plant-optimized requirements.

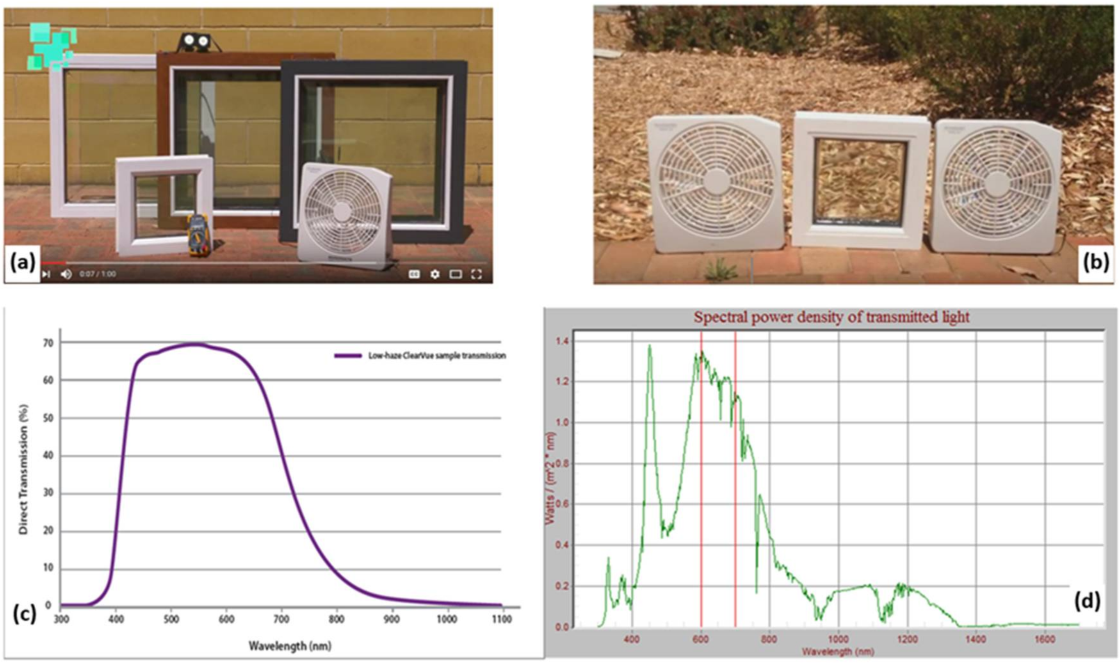

Figure 6. Examples of several earlier solar window design types (a, b); the optical transmission (or transmitted solar energy density) spectra of window systems designed for either the construction (c), or agriculture (d) applications.

The pilot bus-stop installation included six framed solar windows placed vertically along the backside wall of an existing bus stop. Figure 7 shows the front view of this bus stop, which featured also a charge controller and battery storage system, which was being charged either from the combined (parallel-connected PV windows) output, or (previously) from a combination of two Unisolar PVL-72 flexible PV modules rated at 72 W_p each and mounted on the roof of the same bus stop.

Preprints (www.preprints.org) | NOT PEER-REVIEWED | Posted: 2 May 2018 doi:10.20944/preprints201805.0016.v1

Peer-reviewed version available at *Appl. Sci.* **2018**, *8*, 849; doi:10.3390/app8060849

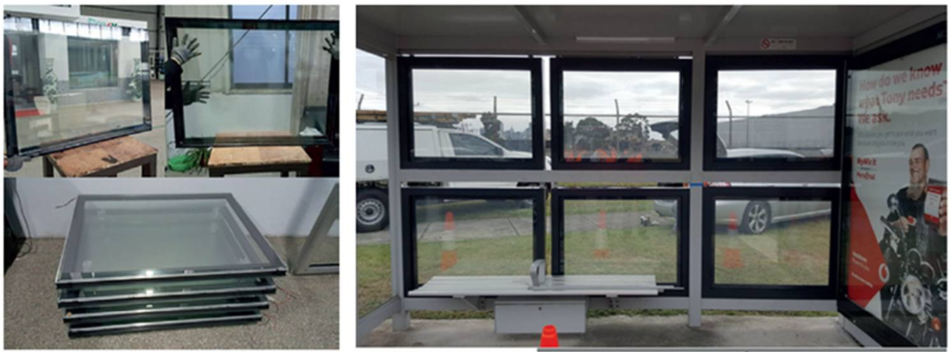

Parameters	Values
Visible Transmission	70% (T direct)
Solar Heat Gain Coefficient	<0.4
Light-to-Solar Gain (LSG + Tvis. % / SHGC)	>1.75
Haze	<4%
Thermal insulation U-value	<2W/(m2*K)
Near-infrared shielding performance (by energy)	>90%
UVA + UVB shielding performance (by energy)	>95%

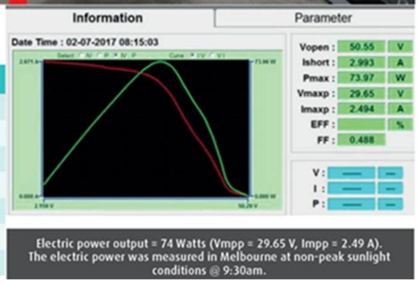

Figure 7. Transparent photovoltaic wall of windows installed into a Port Melbourne bus stop powering an advertising display and lighting appliances. Several unframed PV window modules are also shown during factory assembly process at Qingdao Rocky Ltd (China); shown on left. Several optical transmission and thermal-insulation related parameters and electrical testing data summary are also shown.

The battery-charging current was being measured by the charge controller in real time, and was observed to be at around 4 A, thus replenishing the energy stored in two 12 V parallel-installed batteries, simultaneously with powering all electric loads (consuming 45 W in total), when the system was connected to the wall of solar windows. The total electric power output observed from six solar windows in morning conditions (9:30 am, 07 February 2017, at about 20°C ambient air temperature) reached 74 W, and exceeded that obtained at the same time from two parallel-connected PVL-72 roof-mounted modules (up to 57 W). Figure 8 illustrates the main PV measurement data for both system types.

 doi:10.20944/preprints201805.0016.v1

Peer-reviewed version available at *Appl. Sci.* **2018**, *8*, 849; doi:10.3390/app8060849

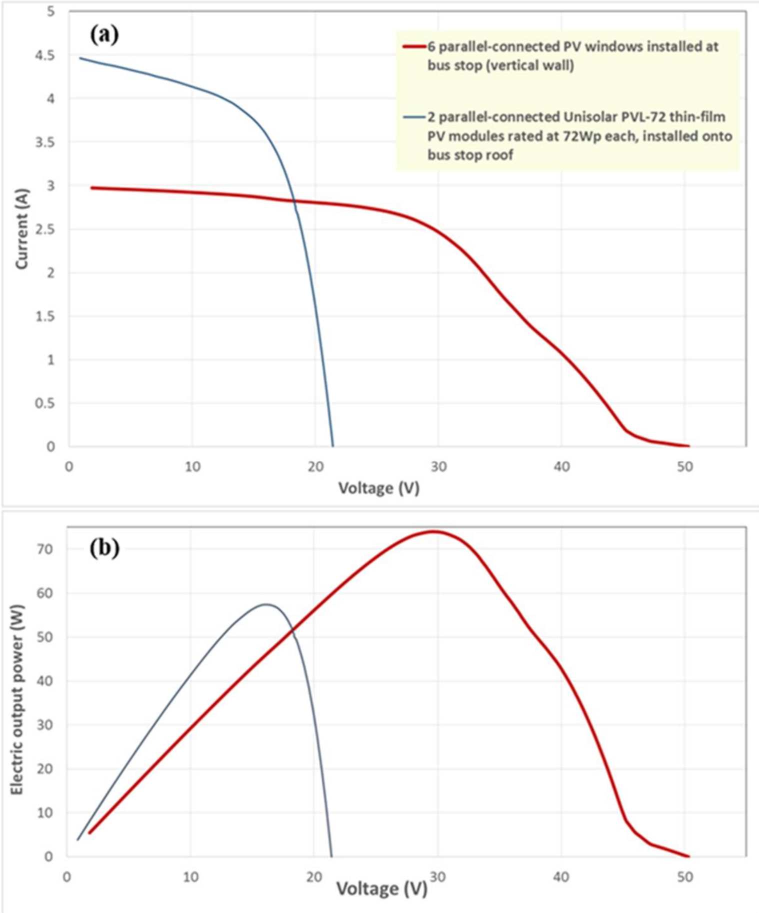

Figure 8. Measured PV I-V curves of a 6-window vertically-oriented bus-stop wall installation and comparison with a reference PV module output. (a) I-V curves of both PV modules measured concurrently in field conditions using PROVA 200A Solar Module Analyzer; (b) the corresponding power-voltage curves data.

The actual measurement time was near 9:30 am on Feb 07, 2017 (when the Sun altitude angle was near 32°, according to the astronomical data from www.suncalc.org). The Sun azimuth angle was 84.8°, and the direction of normal to the vertically-installed wall of PV windows was practically due East, according to Google maps data. A part of bus-stop roof area was overhanging, and shaded some of the solar cell (and also glass) areas from the direct sunlight across the top row of windows. The two parallel-connected Unisolar PVL-72 flexible PV modules (rated at 72 W_P each and covering, in total, 2.24 m^2 of horizontal roof area). Some environmentally-induced contamination was possibly present on top of the active areas of these roof-mounted modules, which might have accounted (together with the weather-related and geometric orientation factors) for some reduction in the measured output of these modules, compared to both the peak ratings and also the expected values – we only observed up to 57.37 W of electric output from the roof-based PV system. Based on this measured electric output, and accounting for the precise geometric orientation of PVL-72 panels with respect to the incoming sunlight and their peak rating, an estimate of the instantaneous direct-beam solar irradiation intensity can be made, resulting in about 752 W/m^2, if any module-area contamination effects or aging-related performance reductions were neglected.

At 9:30 am, near 450 W/m^2 of solar irradiation intensity fell onto the horizontally-oriented surface, according to the published graphs showing the solar irradiation intensities recorded in Melbourne (Caulfield South, http://caulfieldsouthweatherstation.com/charts/solar during the same day). The theoretically maximum radiation intensity falling onto the horizontal roof area would have been (at perfect, AM1.5G peak-weather conditions corresponding to 1000W/m^2 of direct-beam irradiation intensity) near 1000W/m^2*sin (32°), or 530 W/m^2. Therefore, an estimate for the power scaling factor characterizing the weather-dependent system performance applicable to

Preprints (www.preprints.org) | NOT PEER-REVIEWED | Posted: 2 May 2018 doi:10.20944/preprints201805.0016.v1

Peer-reviewed version available at *Appl. Sci.* **2018**, *8*, 849; doi:10.3390/app8060849

measurements made on Feb 07, 2017 can be quantified as W = 450/530 = 0.849. This figure corresponds to 849 W/m^2 of direct-beam irradiation intensity, and significantly exceeds the 752 W/m^2 obtained from pure geometry and rated system performance. Thus, using 849 W/m^2 irradiation intensity can be considered sufficiently conservative for use in our estimates of the peak-weather performance of this PV wall in field conditions, especially considering that some hazy clouds were visually observed during our measurements. The atmospheric path length was also greater than the standard atmospheric path at AM1.5 conditions (due to the Sun altitude angle being 32°).

Therefore, ClearVue 6-window vertical PV wall can be predicted to have demonstrated, at peak weather conditions, approximately the following power output:

P(max, 32° Sun angle, at 1000 W/m^2) = (74W/0.849)*100 = 87.16 W,

where we still haven't accounted for any geometric shading effects induced by the overhanging roof section.

This figure relates to the maximum electric output power expected in real conditions at 32° Sun altitude angle, and would be increased by a further 7-8%, if standard cell-surface temperature of 25°C was used instead (for the NOCT of 40°C), together with temperature coefficient of power (-0.39%/°C). However, for the bus stop application, it is preferable to measure the actual output power at realistic cell-surface temperatures, which are normally in excess of 40°C in Australian summer conditions. Accounting for the sunlight incidence geometry, only about 84.8% of the total direct-irradiation flux cross-section was intercepted by the vertically-positioned windows, for Sun altitude angle of 32°. Thus, we can generate an idealized conditions-based prediction for the maximum electric output rating of this PV wall (when illuminated by 1000W/m^2 sunlight at normal incidence, achieved by tilting the windows backwards, until an optimum output is achieved). Thus, P(max, est. for the optimally-tilted wall angle, at 1000 W/m^2) = 102.8 W.

Considering that the total wall area covered by the six framed windows was about 5.1 m^2, for a maximum predicted power output rating being close to 102.8 W_P, these data corresponds to the maximum electric output per unit optimally-angled PV wall area being up to 20.2 W/m^2. This figure is slightly less than up to 24-26 W/m^2 per unit of framed window area measured with individual windows, due to using conservatively-estimated weather-related data, and the overall performance of a 6-window parallel-connected wall module being limited by its module fill factor (MFF) being slightly smaller than the MFFs of individual (and unshaded) optimally-tilted windows. In all calculations, we also neglected the horizontal-orientation angle effects arising due to the geometric wall normal angle of the bus stop not being aligned perfectly with the Sun azimuth direction. As is practically evident from Figure 9 (taken in slightly cloudier conditions, but only about one hour after making the electrical output measurements), the 849 W/m^2 figure used in irradiation estimates was more than appropriate in terms of conservativeness.

Figure 9. Solar window-powered bus stop installed by Adshel, Inc. (Melbourne, Australia).

Preprints (www.preprints.org) | NOT PEER-REVIEWED | Posted: 2 May 2018 doi:10.20944/preprints201805.0016.v1

Peer-reviewed version available at Appl. Sci. 2018, 8, 849; doi:10.3390/app8060849

Making direct irradiation intensity measurements in field conditions simultaneously with the I-V curve measurements was not a perfect option at the time, due to the cloud-coverage variations taking place even during the data-logging process duration. Several media outlets worldwide, including ABC Australia, have published reports on this trial bus-stop installation of solar windows, in March 2017.

3.2 Future applications in greenhouse agriculture

A small-scale (4m x 4m) pre-prototype of a greenhouse fitted with several solar windows and energy-storage system has also been constructed, in order to provide the initial evaluation-grade data on the ways in which future horticultural greenhouse installations need to be built and designed. Figure 10 shows this initial trial installation in its early stages of construction.

Figure 10. Mini-scale (4m x 4m) prototype greenhouse installation featuring clear solar windows and energy storage/AC conversion technologies used for test-bedding the foundations of relevant greenhouse construction technologies.

A unique combination of features will be tested in a new 300 m² pilot greenhouse installation to be constructed during 2018. We predict achieving a demonstration of significant energy savings in climate control, electricity generation, and possibly even approaching self-sustainable operation mode. Features including on-site water desalination are also expected to be feasible, and crop yield improvements are expected to be demonstrated due to spectrally shaping the illuminating light.

4. Conclusions

In summary, we have successfully achieved a demonstration of a range of practical and visually-clear solar windows, which have been developed at ECU (Perth, Australia) in collaboration with ClearVue Technologies Ltd. Using Avancis CIS PV modules of nominal conversion efficiency 12.3%, the achieved electric power output per unit area of framed large-size (0.85 m²) glass windows was up to about 25 W_p/m^2. With current 15.6 %-efficiency Avancis CIS PV modules, an electric power output exceeding 30 W_p/m^2 can be attained. The principal suitability of these world-first transparent large-scale solar windows for public infrastructure and agricultural applications has been tested and confirmed. Emerging agricultural applications, which are subject to ongoing work, include advanced self-sustainable greenhouses, in which solar windows will shape the transmitted light spectra to the requirements of specific growing plants.

Preprints (www.preprints.org) | NOT PEER-REVIEWED | Posted: 2 May 2018 doi:10.20944/preprints201805.0016.v1

Peer-reviewed version available at *Appl. Sci.* **2018**, *8*, 849; doi:10.3390/app8060849

Author Contributions: All authors (M. V., K. A. and M. N. A.) have contributed to the design of experiments and data collection; M. V. analyzed the data and prepared the manuscript; M. N. A., M. V. and K. A discussed the data and their presentation; M. V. and K. A. reviewed and improved the manuscript.

Funding: This research was funded by the Australian Research Council (grants LP130100130 and LP160101589) and Edith Cowan University.

Acknowledgments: The authors would like to acknowledge the support from ClearVue Technologies Ltd. (www.clearvuepv.com), the Australian Research Council, and Edith Cowan University.

Conflicts of Interest: The authors declare no conflict of interest.

References

1. Li, H.; Wu, K.; Lim, J.; Song, H.-J.; Klimov, V. I. Doctor-blade deposition of quantum dots onto standard window glass for low-loss large-area luminescent solar concentrators. *Nature Energy*. **2016,** 16157, doi: 10.1038/NENERGY.2016.157.
2. Zhao, Y.; Lunt, R. R. Transparent luminescent solar concentrators for large-area solar windows enabled by massive stokes-shift nanocluster phosphors. *Adv. Energy Mater*. **2013**, *3*, 1143–1148.
3. Meinardi, F.; Ehrenberg, S.; Dhamo, L.; Carulli, F.; Mauri, M.; Bruni, F.; Simonutti, R.; Kortshagen U.; Brovelli, S. Highly efficient luminescent solar concentrators based on earth-abundant indirect-bandgap silicon quantum dots. *Nature Photonics*. **2017**, doi: 10.138/NPHOTON.2017.5.
4. Merkx, E. P. J.; Ten Kate, O. M.; Van Der Kolk, E. Rapid optimization of large-scale luminescent solar concentrators: evaluation for adoption in the built environment. *Opt. Express*. **2017**, *25*, A547, https://doi.org/10.1364/OE.25.00A547.
5. Extance, A. The dawn of solar windows, IEEE Spectrum. **2018**, online publication, https://spectrum.ieee.org/energy/renewables/the-dawn-of-solar-windows (sighted in Feb. **2018**).
6. Cocilovo, B.; Hashimura, A.; Tweet, D. J.; Voutsas, T.; Norwood, R. A. Highly transparent light-harvesting window film. *Appl. Opt*. **2015**, 54, 8990–8998.
7. Vasiliev, M.; Alghamedi, R.; Nur-E-Alam, M.; Alameh, K. Photonic microstructures for energy-generating clear glass and net-zero energy buildings. *Sci. Rep*. **2016**, *6*, 31831, doi:10.1038/srep31831.
8. Rezaei, S. D.; Shannigrahi, S.; Ramakrishna, S. A review of conventional, advanced, and smart glazing technologies and materials for improving indoor environment. *Solar Energy Materials and Solar Cells*. **2017**, *159*, 26-51.
9. Dalapati, G. K.; Kushwaha, A. K.; Sharma, M.; Suresh, V.; Shannigrahi, S.; Zhuk, S.; Masudy-Panah, S. Transparent heat regulating (THR) materials and coatings for energy saving window applications: Impact of materials design, micro-structural, and interface quality on the THR performance. *Prog.Mater.Sci*. **2018**, *95*, 45-131.
10. Hanergy Product Manual 201411, Section 1.3 (2014), p. 11, downloaded from www.hanergy.com/en in May **2017**.
11. Sunjoule Product Brochure by Asahi Glass Corp., p. 11, downloaded from http://www.agc-solar.com/agc-solar-products/bipv.html in May **2017**.
12. Cornaro, C.; Basciano, G.; Puggioni, V. A.; Pierro, M. Energy saving assessment of semi-transparent photovoltaic modules integrated into NZEB. *Buildings*, **2017**, *7*, 9.
13. Elinwa, U. K.; Radmehr, M.; Ogbeba, J. E. Alternative energy solutions using BIPV in apartment buildings of developing countries: a case study of North Cyprus. *Sustainability*, **2017**, *9*, 1414.
14. Yang, W.; Deng, H.; Wang, Z.; Zhao, X.; He, S. Performance investigation of the novel solar-powered dehumidification window for residential buildings. *Energies*, **2017**, *10*, 1369.
15. Khan, H. S.; Asif, M.; Mohammed, M. A. Case study of a nearly zero energy building in Italian climatic conditions. *Infrastructures*, **2017**, *2*, 19.
16. Rey-Hernandez, J. M.; Velasco-Gomez, E.; San Jose-Alonso, J. F.; Tejero-Gonzalez, A.; Rey-Martinez, F. J. Energy analysis at a near zero energy building. A case study in Spain. *Energies*, **2018**, *11*, 857.
17. Lee, J.; Park, J.; Jung, H-J.; Park, J. Renewable energy potential by the application of a building integrated photovoltaic and wind turbine system in global urban areas. *Energies*, **2017**, *10*, 2158.
18. Espeche, J. M.; Noris, F.; Lennard, Z.; Challet, S.; Machado, M. PVSITES: Building-integrated photovoltaic technologies and systems for large-scale market deployment. *Proceedings*, **2017**, 1, 690.
19. https://www.forumforthefuture.org/greenfutures/articles/massive-solar-façade-swiss-convention-centre, sighted in April **2018**.
20. Yang, C.; Lunt, R. R. Limits of visibly transparent luminescent solar concentrators. *Adv. Opt. Mater.*, **2017**, *5*, 1600851.

21. Alghamedi, R.; Vasiliev, M.; Nur-E-Alam, M.; Alameh, K. Spectrally-selective all-inorganic scattering luminophores for solar energy-harvesting clear glass windows. *Sci. Rep*. **2014**, 4, 6632, doi:10.1038/srep06632.
22. Marlein, J.; Burgelman, M. Electrical properties of CIGS cells, In Proc. 22nd European Photovoltaic Solar Energy Conference (Milan, Italy), **2007**, 2401–2404.
23. Hughes, M. D.; Borca-Tasciuc, D.-A.; Kaminski, D. A. Highly efficient luminescent solar concentrators employing commercially available luminescent phosphors. *Solar Energy Materials and Solar Cells*, **2017**, *171*, 293-301.
24. El Mouedden, Y.; Alghamedi, R.; Nur-E-Alam, M.; Vasiliev, M.; Alameh, K. Thin film coatings for solar and thermal radiation control prepared by physical vapour deposition. In Proc. 9th International Conference on High Capacity Optical Networks and Enabling Technologies (HONET) **2012**, doi: 10.1109/HONET.2012.6421440.
25. Topič, M.; Geisthardt, R.M.; Sites, J.R. Performance limits and status of single-junction solar cells with emphasis on CIGS. *IEEE J. Photovolt*., **2015**, *5*, 360-365.